行政院國家科學委員會補助專題研究計畫 ■成果報告 □期中進度報告

近紅外光感測器用之高靈敏度共軛高分子/奈米顆粒複合材料

High Sensitivity conjugated polymer/ nanoparticle Nanocomposite for Near IR Sensor Applications

計畫類別：■個別型計畫　□整合型計畫
計畫編號：NSC 97－2221－E－009－006－MY3
執行期間：98 年 8 月 1 日至 99 年 7 月 31 日

執行機構及系所：交通大學材料科學與工程學系

計畫主持人：韋光華
共同主持人：
計畫參與人員：韋光華、郭芝吟、蘇明鑫、林惠妮、許毓倩

成果報告類型(依經費核定清單規定繳交)：□精簡報告　■完整報告

本計畫除繳交成果報告外，另須繳交以下出國心得報告：
□赴國外出差或研習心得報告
□赴大陸地區出差或研習心得報告
□出席國際學術會議心得報告
□國際合作研究計畫國外研究報告

處理方式：除列管計畫及下列情形者外，得立即公開查詢
□涉及專利或其他智慧財產權，□一年□二年後可公開查詢

中　華　民　國 99 年　7 月　29 日

中、英文摘要

關鍵詞: 硒化鉛量子點、光伏元件、電洞傳輸層、PEDOT:PSS、X 光反射
keywords : PbSe quantum dots, photovoltaic device, hole transport layer, PEDOT:PSS, X-ray reflectivity

探討 PEDOT:PSS 電洞傳輸層對 PbSe 量子點多層膜光伏特元件之影響。藉由穿透式式電子顯微鏡與 X-ray reflectivity 量測得知，添加 PEDOT:PSS 可使 PbSe 量子點多層膜光伏特元件表面型態較為平滑。此外，經由光伏特元件之電流-電壓特性曲線量測發現，隨著 PbSe 量子點第一激發吸收波長的增加，粒徑變大，元件之開放電壓有變小的趨勢，而添加 PEDOT:PSS 使得 PbSe 薄膜元件的開放電壓有增加的現象，且太陽能元件轉換效率從 1.5%提升至 2.4%，比沒有添加 PEDOT:PSS 之元件增加了 60%。根據量測外部量子效率，得知此元件在可見光與紅外光區皆有光電流響應。在元件穩定性方面，分別持續照射模擬太陽光數百分鐘，當效率衰減至原先之 80%時，添加 PEDOT:PSS 之元件所經歷的時間為沒有 PEDOT:PSS 之元件的六倍，得知 PEDOT:PSS 可使得 PbSe 量子點多層膜光伏特元件維持長時間的元件壽命。

A thin poly(3,4-ethylenedioxythiophene):poly(styrene sulfonate) (PEDOT:PSS) hole transport layer enhances the AM1.5 power conversion efficiency of a PbSe quantum dot (QD)–containing photovoltaic device to 2.4%, from 1.5% for a standard PbSe QD device, a relative increase of 60%. Synchrotron X-ray reflectivity measurements revealed that the roughness of the interfaces between the various layers decreased dramatically in the presence of the PEDOT:PSS layer. In addition, the device life time under continuous simulated AM1.5 irradiation (100 mW cm^{-2}), measured in terms of the time required to reach 80% of the normalized efficiency, for the PbSe QD device incorporating the PEDOT:PSS hole transport layer was six times longer than that of the standard PbSe QD device.

報告內容

1. Introduction

Fabricating photovoltaic devices using solution-processed materials has many potential benefits, particularly for the rapid and economical preparation of flexible, large-area devices. Solution-processing of organic polymers,[1,2] inorganic semiconductors,[3–5] and organic/inorganic hybrids[6–9] has been adopted widely. One example of the use of conjugated polymers is in the preparation of heterojunction photovoltaic devices, which have achieved solar conversion efficiencies greater than 6%.[10] Nevertheless, because composites of low-bandgap conjugated polymers and fullerene derivatives remain active only at wavelengths from 300 to 800 nm, they fail to harvest most of the radiation in the infrared (IR) spectral region. By virtue of the quantum size effect, colloidal quantum dots (QDs) of Pb salts have absorption characteristics that can be tuned throughout the IR spectrum.[11–13] Furthermore, colloidal Pb-salt QDs can potentially undergo multiple exciton generation,[14,15] the generation of more than one electron/hole pair. If multiexciton formation, dissociation, and charge collection were all efficient events, the resulting enhanced photocurrent would lead to an increase in the solar energy conversion efficiency.[16] Hence, the development of Pb-salt colloidal QDs for use in optoelectronic devices has emerged recently as an active area of investigation.[17–20]

Using a layer-by-layer (LBL) technique—one that involves alternate (i) dip-coating or spin-coating of QDs onto a patterned indium tin oxide (ITO) substrate and (ii) exposing the QD films to a bidentate ligand to can effectively remove the long, insulating oleate ligands from the as-synthesized PbSe QDs—has resulted in increased conductivities of PbSe QD films and excellent photovoltaic performance.[4,5,21] The first example of the use of LBL processing of PbSe QDs to form a double-layer device structure led to an AM1.5 power conversion efficiency (PCE) of 1.1%.[22] Later, it was demonstrated that PbSe QD photovoltaic devices exhibit superior performance, with AM1.5 PCEs of ca. 2.1%.[23] Subsequently, large improvements in the open-circuit voltages (V_{oc}) were obtained when combining PbS_xSe_{1-x} QDs[24] or PbSe QD/ZnO heterojunctions[25,26] with the LBL technique, resulting in higher PCEs.

Because a completed QD active layer can feature more than 20 layers processed individually using the LBL technique, the quality of the interfaces between these layers is critical for good charge transport to occur across them and to achieve good device performance.[27] Moreover, the alignment between the valence band of the QDs and the work function of the metal oxide anode will affect the open-circuit voltage of the photovoltaic devices. Hence, a high-quality interface must exist between the anode of the device and the first QD layer. In this study, we introduced a thin (ca. 20 nm) poly(3,4-ethylenedioxythiophene): poly(styrene sulfonate) (PEDOT:PSS) hole transport layer into the interface between a tri-layered PbSe QD active layer and ITO substrate to improve the interfacial smoothness and band alignment and, thereby, enhance the device's photovoltaic performance and life time. The fabrication of these devices is described in the Experimental section; the device structure comprised an ITO anode, Al/Ca cathode, and PbSe QD

active layer, with or without a PEDOT:PSS layer.

2. Results and Discussion

Figure 1 displays the current density–voltage characteristics of a device incorporating a 95-nm-thick layer of 4.5-nm-diameter PbSe QDs under AM 1.5G conditions (100 mW cm^{-2}, 25 °C) and in the dark. The dark current curves of the devices reveal a turn-on voltage of ca. 0.1 V. The PCE for the device incorporating a 20-nm-thick PEDOT:PSS layer was 2.4%, up from 1.5% for the standard device. This increase of 60% in the PCE of the device incorporating the PEDOT:PSS layer, relative to that of the standard device, resulted from increases in the values of both V_{oc} and the short-circuit current density (J_{sc}). The value of V_{oc} of 0.24 V for the device featuring the PEDOT:PSS layer was ca. 33% greater than that of 0.18 V for the standard device. The increase in V_{oc} can be explained in terms of the superior interfacial energy level offset in the device in the presence of the PEDOT:PSS layer than in its absence. Because the incorporated PEDOT:PSS layer has a work function of 5.1 eV, positioned between the valence band of 5.3 eV[25,28] for the 4.5-nm-diameter PbSe QDs and the work function of 4.8 eV of the ITO electrode, this kind of band energy alignment facilitates the transport of dissociated holes to the anode. The inset of **Figure 1** displays the energy band diagram for the various layers in the device. The value of J_{sc} increased to 21.9 mA cm^{-2} for the device incorporating the PEDOT:PSS layer from 18.0 mA cm^{-2} for the unmodified device, an increase of ca. 20%, presumably because of superior interfacial contacts and, therefore, improved carrier transport between the PbSe QDs and the PEDOT:PSS layer. The fill factors (FFs) of these two devices, however, were similar. **Table 1** lists the current density–voltage characteristics of the PbSe QD device, incorporating a PEDOT:PSS intermediate layer, under 100 mW cm^{-2} solar AM1.5G illumination.

Figure 2a presents a cross-sectional TEM image of a device incorporating a PEDOT:PSS layer (thickness: 20 nm) and a PbSe QD active layer (thickness: 95 ± 5 nm); two interfaces are clearly evident in the active layer (i.e., PbSe-1–PbSe-2 and PbSe-2–PbSe-3). The thickness of this active layer (ca. 95 nm) is close to the optimal value for PbSe QDs devices.[23–25] Closer examination on the TEM image of the ITO/PEDOT:PSS/PbSe QDs/Ca/Al device structure revealed that the PbSe QDs formed a dense layer that was in intimate physical contact with the PEDOT:PSS layer. The PEDOT:PSS layer apparently provided a smooth transition from the rough ITO surface to the PbSe QD layer. The formation of a smooth active layer, an important feature for efficient device operation, presumably resulted from strong polar interactions between the PbSe QDs and the PEDOT:PSS layer.[29] Furthermore, the interfacial roughness among the PbSe QD layer, the incorporated PEDOT:PSS layer, and the ITO substrate could be determined quantitatively using synchrotron X-ray reflectivity (XRR) measurements. **Figure 2b** presents XRR curves of the PbSe QD films on ITO substrates, in the presence and absence of the PEDOT:PSS layer. The curve of the device incorporating the PEDOT:PSS layer exhibits

oscillating behavior between 0.3 and 1.0 nm^{-1}; that of the device lacking a PEDOT:PSS layer appears to be much smoother, providing further evidence that the PEDOT:PSS layer reduced the interfacial roughness of this device. **Table 2** lists the interfacial roughness parameters obtained from curve-fitting the XRR data.[30] The device prepared without a PEDOT:PSS layer between the ITO substrate and the PbSe layer had a roughness, $\sigma_{ITO/PbSe-1}$, of 2.9 nm. After incorporating a PEDOT:PSS layer on the ITO substrate, the roughness of the interface between the PEDOT:PSS and PbSe QD layers, $\sigma_{PEDOT:PSS/PbSe-1}$, became 1.0 nm, almost a three-fold improvement with respect to that of the original ITO–PbSe QD interface. Furthermore, the fitting results revealed that the PEDOT:PSS layer not only reduced the interfacial roughness of the ITO/PbSe QD substrate but also smoothed the interface between the individually spun PbSe QD layers; the value of $\sigma_{PbSe-1/PbSe-2}$ decreased to 2.8 nm in the presence of PEDOT:PSS layer, from 5.0 nm in its absence.

Figure 3a presents current density–voltage plots of PbSe QDs devices featuring various QD sizes in the presence of the PEDOT:PSS layer; **Table 3** lists the photovoltaic properties of these PbSe QD devices. The value of V_{oc} of the device decreases from 0.24 to 0.14 V, while the value of J_{sc} decreased from 21.9 to 17.7 mA cm^{-2}, upon increasing the size of the PbSe QDs from 4.5 to 6.0 nm. The decrease in V_{oc} upon increasing the QD size was due mainly to the corresponding rising of the valence band and the narrowing of the band gap of the PbSe QDs. **Figure 3b** presents the values of V_{oc} of the devices incorporating different sizes of PbSe QDs plotted with respect to their band gaps (E_g), which we estimated from their sizes as reported in the literature.[25,28] We observe linear behavior in the plots of V_{oc} against E_g for the devices containing and lacking the PEDOT:PSS layer. For the devices incorporating a PEDOT:PSS layer, the approximately linear behavior between the values of V_{oc} and E_g of the PbSe QDs can be described using the empirical equation

$$V_{oc} = 0.65(E_g / e) - 0.30V \quad (1)$$

where e is the charge of an electron. The slope (0.65) of the line is close to the value reported in the literature for devices containing similar QDs.[26] The decrease in J_{sc} of the device was caused presumably by increased interfacial roughness when the size of the PbSe QDs increased.

Figure 4 presents external quantum efficiency (EQE) curves for the ITO/PbSe QDs/Ca/Al (standard) and ITO/PEDOT:PSS/PbSe QDs/Ca/Al devices in the wavelength region from 300 to 1800 nm. The device incorporating PEDOT:PSS exhibits a larger EQE than that of the standard device from 360 to 1000 nm, covering the entire visible light range and a small portion of near-IR range. At 650 nm, for instance, the EQE reached 57% for the device containing the PEDOT:PSS layer, compared with 46% for the standard device. The theoretical short-circuit current densities obtained after integrating the EQE curves for the device incorporating PEDOT:PSS and for the standard device were 21.6 and 17.9 mA cm^{-2}, respectively; these values are close to those (21.9 and 18.0 mA cm^{-2}, respectively) obtained directly from the *I–V* curves, confirming the accuracy of

our measurements. **Figure 5** reveals that an approximately linear relationship exists between the short-circuit current density and the incident light intensity over the range from 0 to 100 mW cm^{-2}, suggesting that this type of device might also find use as a photodetector.

Next, we tested the durability of our solar device under simultaneous and continuous AM1.5G illumination and current–voltage scanning. Because PbSe QD–based devices are air-sensitive, with instantaneous degradation having been reported upon their exposure to air,[19,23] all of our devices were packaged before being measured under ambient conditions. **Figure 6** reveals that the stability of the PCE of the device incorporating the PEDOT:PSS layer was substantially greater relative to that of the device lacking the PEDOT:PSS layer. In particular, the device life times, measured in terms of the time required to reach 80% of the normalized efficiency, for the standard PbSe QD device and the PbSe QD device incorporating the PEDOT:PSS layer were 20 and 120 min, respectively, a six-fold improvement for the latter. Notably, the device incorporating the PEDOT:PSS layer exhibited almost constant values of J_{sc} and FF during its first 60 min of operation; in contrast, its value of V_{oc} decreased gradually.

3. Conclusions

We have prepared photovoltaic devices featuring a PEDOT:PSS hole transport layer and three individually deposited PbSe QD layers. The PbSe photovoltaic devices incorporating the PEDOT:PSS layer exhibited enhanced AM1.5 PCEs relative to those of devices lacking the hole transport layer, with an enhancement factor of 60%. The roughness of the interface between the PEDOT:PSS and PbSe QD layers was almost three times less than that of the original ITO–PbSe QD interface, as measured using X-ray reflectivity. Hence, the presence of the PEDOT:PSS layer not only provided a smoother interface between the PbSe QD layers and the ITO substrate but also resulted in enhanced open-circuit voltages. In addition, the presence of the PEDOT:PSS hole transport layer prolonged the life time, as measured in terms of the time required to reach 80% of the normalized efficiency, of the PbSe QD solar device by six-fold, suggesting that this approach improves the performance of PbSe QD photovoltaic devices.

4. Experimental

Materials: Lead(II) oxide (PbO, 99.99%) was obtained from Alfa Aesar. Selenium (Se, 99.9%), oleic acid (OA, tech. 90%), trioctylphosphine (TOP, tech. 90%), 1-octadecene (ODE, tech. 90%), butylamine (BA, 99.5%), and 1,2-ethanedithiol (EDT, 98%) were purchased from Sigma–Aldrich. Octane (HPLC-grade) and acetonitrile (anhydrous) were obtained from TEDIA. Methanol (anhydrous), toluene (anhydrous), and isopropanol (anhydrous) were obtained from J. T. Baker.

PbSe QDs: The QDs were synthesized using standard Schlenk line techniques under an Ar

flow; the PbSe used in this study was synthesized according to the method reported by Yu et al [31]. PbO (0.8920 g, 4.000 mmol), oleic acid (2.825 g, 10.00 mmol), and ODE (12.83 g) were stirred together in a three-neck flask and heated at 160 °C under continuous Ar flow for 30 min to obtain a colorless, clear solution. At this temperature, 10% Se-TOP solution (6.4 g) was quickly injected into the solution, dropping the temperature to ca. 150 °C for the growth process. After allowing the reaction to proceed for 30–120 s, the mixture was quenched by placing it in a water/ice bath for 1 min. The colloidal QDs were isolated from the growth mixture through repeated precipitations with methanol prior to being dispersed in toluene, vacuum-dried, and stored in a glove box. **Figure S1** (Supporting Information) displays TEM images of the synthesized PbSe QDs.

BA Ligand Exchange: The ligand exchange process was performed in a N_2-filled glove box, following the method reported by Konstantatos et al [32]. The as-synthesized PbSe colloidal QDs were redispersed (to 50 mg mL^{-1}) in anhydrous BA and stirred continuously for 3 days. The resultant QDs were precipitated with anhydrous isopropanol and redispersed in anhydrous octane (80 mg mL^{-1}) for device fabrication. This ligand exchange on the PbSe QDs, albeit completed only partially [17, 33], was designed to obtain better film surface structures than that of PbSe QDs without the ligand exchange after spin-coating; see **Figure S2** (Supporting Information).

Device Fabrication: The patterned ITO on the glass substrate (5 Ω $sq.^{-1}$, Merck) was cleaned through sequential ultrasonic treatment (30 min) with 2% detergent, methanol, acetone, and isopropanol and then dried under a flow of N_2. PEDOT:PSS (Baytron P VP AI 4083) was then spin-coated on the ultraviolet ozone–treated ITO. After annealing the PEDOT:PSS film at 150 °C for 10 min, the PbSe QDs in anhydrous octane were spin-coated onto the PEDOT:PSS layer on the patterned ITO; the samples were then soaked in 0.01 M EDT in anhydrous acetonitrile for several seconds to enhance the film conductivity. The fabrication of the photovoltaic devices involved several steps: (1) the BA-treated PbSe QDs in octane were spin-coated on the PEDOT:PSS layer that had previously been deposited and dried on the ITO electrode; (2) the whole sample, with its surface PbSe QD layer, was treated with 0.01M EDT; (3) the whole sample was rinsed with anhydrous acetonitrile and octane to remove residual free-standing EDT molecules; (4) the treated sample was dried under a stream of N_2. The resulting PbSe QDs layer is referred herein as PbSe-1. A second layer of EDT-treated PbSe QDs (PbSe-2) was prepared on top of the first by repeating this process. Finally, a third layer of PbSe QDs (PbSe-3) was deposited; together, these three individually spun PbSe QD layers served as the active layer. **Figure S3** (Supporting Information) presents the Fourier transform IR spectrum of the spin-coated PbSe QD films on the ITO substrates before and after treatment with EDT. The sharp decreases in the intensities of the C–H and COO^- signals after EDT treatment indicated that most of the oleate ligands on the PbSe QDs had been removed, because thiol–Pb bonds are much stronger than amine–Pb bonds [4]. The thickness of the PbSe QD layer was measured using a Dektak

profilometer. Finally, 20-nm Ca and 100-nm Al top electrodes were deposited onto all of the samples at ca. 10^{-7} torr by thermal evaporation through a shadow mask. Four devices were fabricated on each substrate, each with an active area of 0.04 cm^2.

Characterization: Current density–voltage characteristics of the PbSe QD devices were measured under simulated AM1.5G irradiation (100 mW cm^{-2}) using a Xe lamp–based Newport 66902 150-W solar simulator equipped with a Keithley 236 source measurement unit. The sweeps were performed between +1 and –1 V, with a step size of 0.01 V. For solar cell measurements, the spectrum of the solar simulator was calibrated as follows: A PV-measurement (PVM-154) mono-Si solar cell (NREL calibrated) and a Si photo diode (Hamamatsu S1133) were used to check the irradiation of the exposed area (100 mW cm^{-2}). The mismatch factor (M = 1.34) was obtained by using the PVM-154 cell as the reference cell and the fabricated devices as test cells and recording spectra from 300 to 900 nm at intervals of 10 nm. The PVM-154 cell was combined with a KG-5 filter (350–700 nm passed, Newport) to simulate a reference solar cell having spectral responsivity from 350 to 700 nm. The calibration was based on the IEC-69094-1 spectrum. EQE data were recorded with respect to the Optosolar SPF50 spectrum response. A Si reference cell was used to calibrate the wavelengths of light from 300 to 1060 nm, and a Ge reference cell from 1060 to 1800 nm.

Fourier transform infrared (FTIR) spectra were recorded at room temperature using a Perkin–Elmer Spectrum100 instrument. Scanning electron microscopy (SEM) images was acquired using a JEOL JSM-6500F FESEM apparatus operated at accelerating voltages ranging from 5.0 to 15 kV. Transmission electron microscopy (TEM) images were recorded using an FEI Tecnai G^2 instrument operated at 200 keV. Synchrotron X-ray reflectivity (XRR) analyses were performed at the wiggler beamline BL-17B1 using an eight-circle diffractometer at the National Synchrotron Radiation Research Center (NSRRC), Hsinchu, Taiwan; the photon energy was 8 keV and the flux was estimated to be 10^{11} photons s^{-1}. The use of two pairs of slits between the sample and the detector provided a typical wave-vector resolution of ca. 0.001 nm^{-1} in the vertical scattering plane.

[1] J. Y. Kim, K. Lee, N. E. Coates, D. Moses, T. Q. Nguyen, M. Dante, A. J. Heeger, Science 2007, 317, 222–225.

[2]a) L. M. Chen, Z. Hong, G. Li, Y. Yang, Adv. Mater. 2009, 21, 1434–1449. b) Y. T. Chang, S. L. Hsu, M. H. Su, K. H. Wei, Adv. Mater. 2009, 21, 2093–2097.

[3] I. Gur, N. A. Fromer, M. L. Geier, A. P. Alivisatos, Science 2005, 310, 462–465.

[4] J. Tang, X. Wang, L. Brzozowski, D. A. R. Barkhosue, R. Debnath, L. Levina, E. H. Sargent, Adv. Mater. 2010, 22, 1–5.

[5] D. V. Talapin, C. B. Murray, Science 2005, 310, 86–89.

[6] S. A. McDonald, G. Konstantatos, S. Zhang, P. W. Cyr, E. J. D. Klem, L. Levina, E. H. Sargent, Nat. Mater. 2005, 4, 138–142.

[7] N. Cho, K. R. Choudhury, R. B. Thapa, Y. Sahoo, T. Ohulchanskyy, A. N. Cartwright, K. S. Lee, P. N. Prasad, Adv. Mater. 2007, 19, 232–236.

[8] H. Y. Chen, M. K. F. Lo, G. Yang, H. G. Monbouquette, Y. Yang, Nature Nanotechnology 2008, 3, 543–547.

[9] Z. Tan, T. Zhu, M. Thein, S. Gao, A. Cheng, F. Zhang, C. Zhang, H. Su, J. Wang, R. Henderson, J. Hahm, Y. Yang, J. Xu, Appl. Phys. Lett. 2009, 95, 063510.

[10] a) J. Hou, H. Y. Chen, S. Zhang, R. I. Chen, Y. Yang, Y. Wu, G. Li, J. Am. Chem. Soc. 2009, 131, 15586–15587. b) Y. Liang, Z. Xu, J. Xia, S. T. Tsai, Y. Wu, G. Li, C. Ray, L. Yu, Adv. Mater. 2010, DOI: 10.1002/adma.200903528.

[11] M. A. Hines, G. D. Scholes, Adv. Mater. 2003, 15, 1844–1849.

[12] R. Koole, G. Allan, C. Delerue, A. Meijerink, D. Vanmaekelbergh, A. J. Houtepen, Small 2008, 4, 127–133.

[13] K. Roy Choudhury, Y. Sahoo, T. Y. Ohulchanskyy, P. N. Prasad, Appl. Phys. Lett. 2005, 87, 073110.

[14] M. C. Beard, A. G. Midgett, M. Law, O. E. Semonin, R. J. Ellingson, A. J. Nozik, Nano Lett. 2009, 9, 836–845.

[15] V. Sukhovatkin, S. Hinds, L. Brzozowski, E. H. Sargent, Science 2009, 324, 1542–1544.

[16] R. D. Schaller, V. I. Klimov, Phys. Rev. Lett. 2004, 92, 186601.

[17] J. Tang, X. Wang, L. Brzozowski, D. A. R. Barkhouse, R. Debnath, L. Levina, E. H. Sargent, Adv. Mater. 2010, 22, 1398–1402.

[18] H. Lee, H. C. Leventis, S. J. Moon, P. Chen, S. Ito, S. A. Haque, T. Torres, F. Nüesch, T. Geiger, S. M. Zakeeruddin, M. Grätzel, Md. K. Nazeeruddin, Adv. Funct. Mater. 2009, 19, 2735–2742.

[19] T. Rauch, M. Böberl, S. F. Tedde, J. Fürst, M. V. Kovalenko, G. Hesser, U. Lemmer, W. Heiss, O. Hayden, Nature Photonics 2009, 3, 332–336.

[20] M. S. Kang, J. Lee, D. J. Norris, C. D. Frisbie, Nano Lett. 2009, 9, 3848–3852.

[21] J. M. Luther, M. Law, Q. Song, C. L. Perkins, M. C. Beard, A. J. Nozik, ACS Nano 2008, 2, 271–280.

[22] G. I. Koleilat, L. Levina, H. Shukla, S. H. Myrskog, S. Hinds, A. G. Pattantyus-Abraham, E. H. Sargent, ACS Nano 2008, 2, 833–840.

[23] J. M. Luther, M. Law, M. C. Beard, Q. Song, M. O. Reese, R. J. Ellingson, A. J. Nozik, Nano Lett. 2008, 8, 3488–3492.

[24] W. Ma, J. M. Luther, H. Zheng, Y. Wu, A. P. Alivisatos, Nano Lett. 2009, 9, 1699–1703.

[25] J. J. Choi, Y. F. Lim, M. B. Santiago-Berrios, M. Oh, B. R. Hyun, L. Sun, A. C. Bartnik, A. Goedhart, G. G. Malliaras, H. D. Abruña, F. W. Wise, T. Hanrath, Nano Lett. 2009, 9, 3749–3755.

[26] K. S. Leschkies, T. J. Beatty, M. S. Kang, D. J. Norris, E. S. Aydil, *ACS Nano* **2008**, 3, 3638-3648.

[27] G. Li, V. Shrotriya, J. Huang, Y. Yao, T. Moriarty, K. Emery, Y. Yang, *Nat. Mater.* **2005**, 4, 864-868.

[28] D. Cui, J. Xu, T. Zhu, G. Paradee, S. Ashok, M. Gerhold, *Appl. Phys. Lett.* **2006**, 88, 183111.

[29] D. M. N. M. Dissanayake, R. A. Hatton, T. Lutz, R. J. Curry, S. R. P. Silva, *Nanotechnology* **2009**, 20, 245202.

[30] L. G. Parratt, *Phys. Rev.* **1954**, 95, 359-369.

[31] W. W. Yu, J. C. Falkner, B. S. Shih, V. L. Colvin, *Chem. Mater*. **2004**, 16, 3318-3322.

[32] G. Konstantatos, I. Howard, A. Fischer, S. Hoogland, J. Cliffod, E. Klem, L. Levina, E. H. Sargent, *Nature* **2006**, 442, 180-183.

[33] M. V. Kovalenko, D. V. Talapin, M. A. Loi, F. Cordella, G. Hesser, M. I. Bodnarchuk, W. Heiss, *Angew. Chem. Int. Ed.* **2008**, 47, 3029-303

Table 1. Performance parameters of PbSe QD devices incorporating a PEDOT:PSS intermediate layer, under solar illumination.

Device structure	V_{oc} [a] (V)	J_{sc} [b] (mA cm^{-2})	FF[c] (%)	η[d] (%)
ITO/PbSe/Ca/Al	0.19	18.0	44.0	1.5
ITO/PEDOT:PSS/PbSe/Ca/Al	0.24	21.9	45.5	2.4

[a] V_{oc}: Open-circuit voltage. [b] J_{sc}: Short-circuit current density. [c] FF: Fill factor. [d] η: PCE. Solar: AM1.5G (100 mW cm^{-2}).

Table 2. Interfacial roughness data obtained by fitting the XRR curves of various layer structures.

ITO/PbSe QDs structure interfacial roughness	nm	ITO/PEDOT:PSS/PbSe QDs structure interfacial roughness	nm
$\sigma_{ITO/PbSe-1}$	2.9	$\sigma_{ITO/PEDOT:PSS}$	3.1
–	–	$\sigma_{PEDOT:PSS/PbSe-1}$	1.0
$\sigma_{PbSe-1/PbSe-2}$	5.0	$\sigma_{PbSe-1/PbSe-2}$	2.8

Table 3. Performance parameters of devices featuring PbSe QDs of various average diameters and incorporating a PEDOT:PSS intermediate layer, under solar illumination.

PbSe QD size (nm)	V_{oc} (V)	J_{sc} (mA cm^{-2})	FF (%)	η (%)
6.0	0.14	17.7	34.9	0.86
5.5	0.17	17.8	39.0	1.18
5.2	0.20	18.5	38.2	1.41
4.8	0.23	19.7	43.4	1.97
4.5	0.24	21.9	45.5	2.40

Figure Captions

Figure 1. Current density–voltage characteristics of 4.5-nm-diameter PbSe QD devices incorporating a PEDOT:PSS intermediate layer, recorded in the dark and under solar illumination (100 mW cm^{-2}). Inset: Energy-level diagram for a PbSe QD photovoltaic device.

Figure 2. (a) TEM cross-sectional image of the ITO/PEDOT:PSS/PbSe QD film/Ca/Al device stack; scale bar: 50 nm. (b) Synchrotron X-ray reflectance for structures incorporating PbSe QD layers, prepared with and without a PEDOT:PSS thin layer.

Figure 3. (a) Current density–voltage plots of devices incorporating a PEDOT:PSS layer and PbSe QDs of various average dameters. (b) Open-circuit voltages (V_{oc}) plotted with respect to the diameter of the PbSe QDs and the band gap energy (E_g) of the devices prepared with and without a PEDOT:PSS layer.

Figure 4. EQE spectra of PbSe QD devices prepared with and without a PEDOT:PSS layer.

Figure 5. Photocurrent density (J_{sc}) plotted with respect to the intensity of solar light for the PbSe QD device prepared with and without a PEDOT:PSS layer.

Figure 6. Values of (a) PCE, (b) V_{oc}, J_{sc}, and FF, measured as a function of time and normalized with respect to their initially measured values, for devices prepared with and without a PEDOT:PSS intermediate layer, illuminated continuously under simulated AM1.5G irradiation (100 mW cm^{-2}).

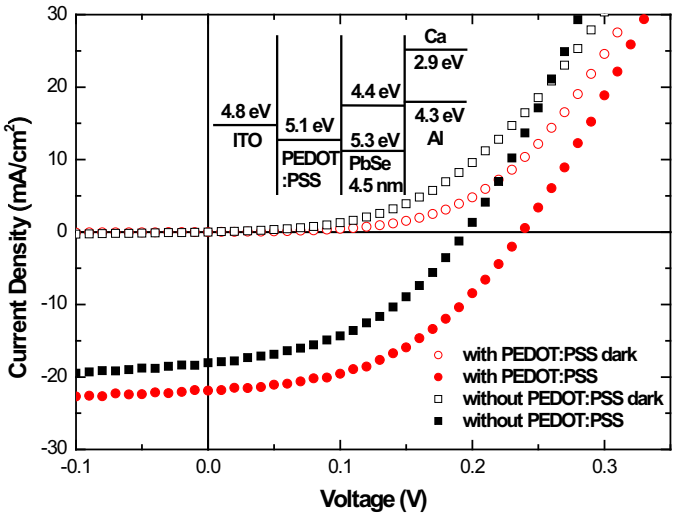
Current Density (mA/cm^2)
Voltage (V)
30
20
10
0
-10
-20
-30
-0.1
0.0
0.1
0.2
0.3
4.8 eV
ITO
5.1 eV
PEDOT
:PSS
4.4 eV
5.3 eV
PbSe
4.5 nm
Ca
2.9 eV
4.3 eV
Al
with PEDOT:PSS dark
with PEDOT:PSS
without PEDOT:PSS dark
without PEDOT:PSS

Figure 1

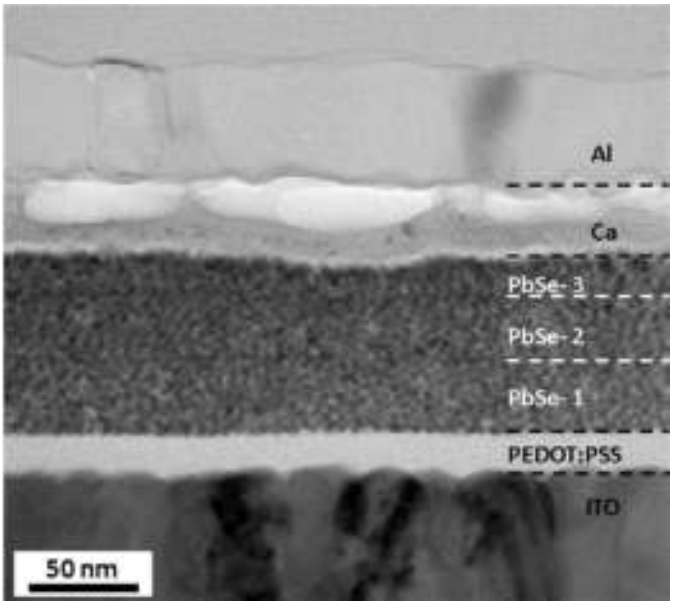

Figure 2a

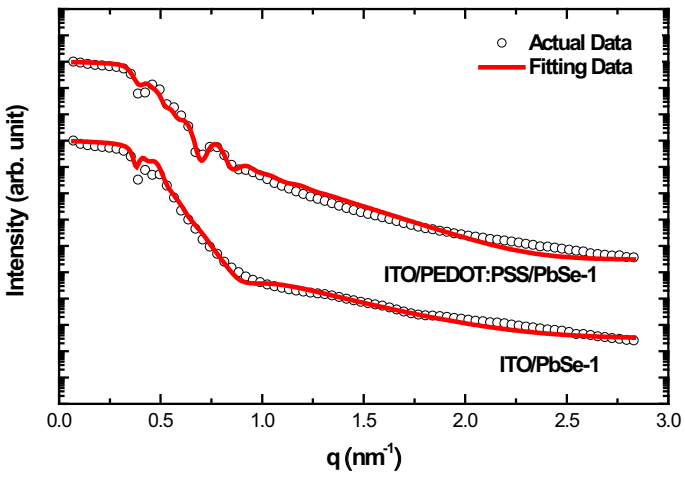

Figure 2b

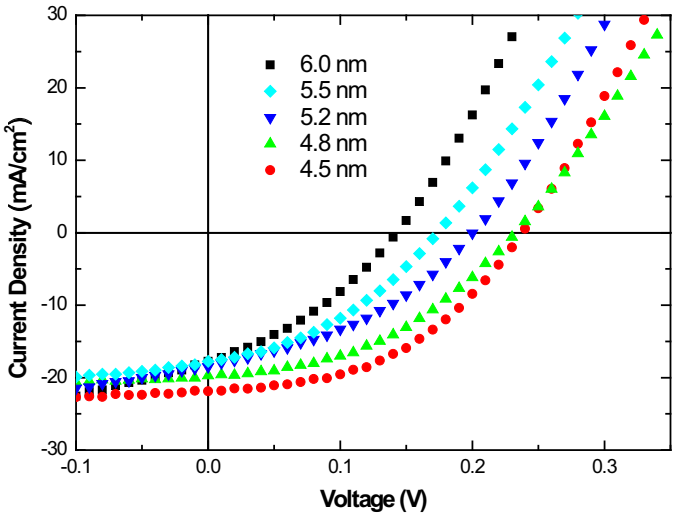

Figure 3a

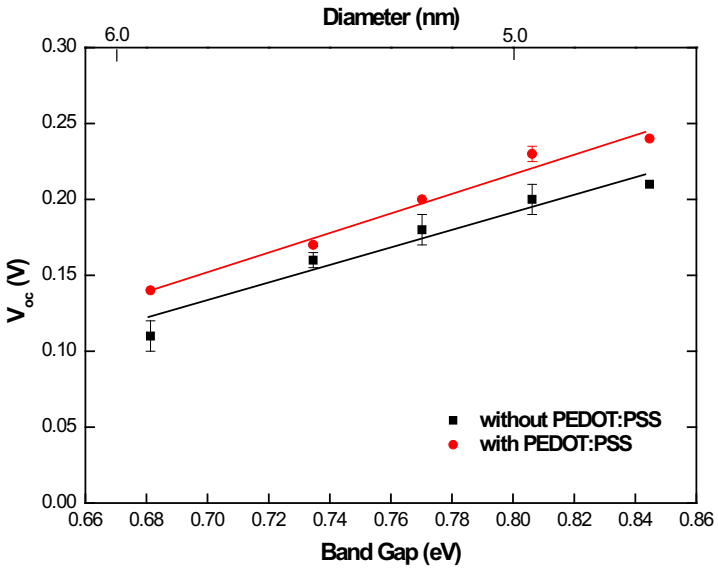

Figure 3b

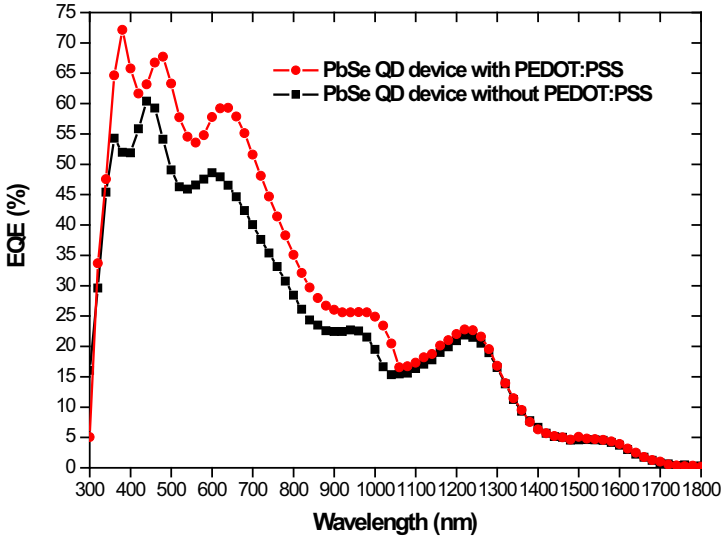
PbSe QD device with PEDOT:PSS
PbSe QD device without PEDOT:PSS
EQE (%)
Wavelength (nm)
0
5
10
15
20
25
30
35
40
45
50
55
60
65
70
75
300
400
500
600
700
800
900
1000
1100
1200
1300
1400
1500
1600
1700
1800

Figure 4

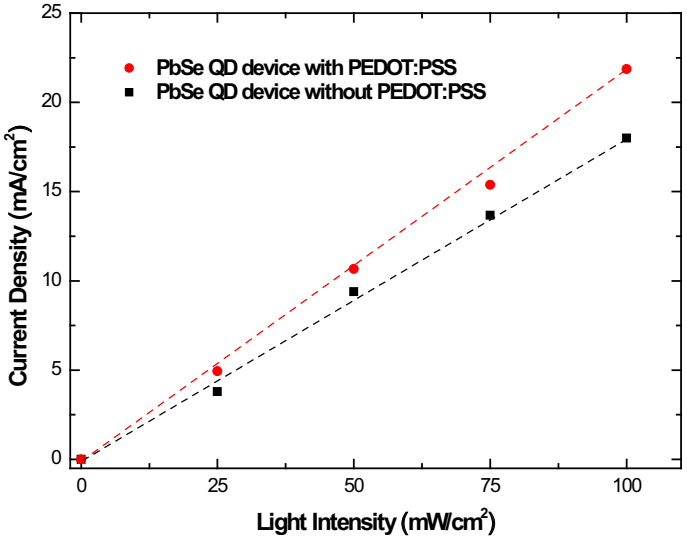
PbSe QD device with PEDOT:PSS
PbSe QD device without PEDOT:PSS
Current Density (mA/cm^2)
Light Intensity (mW/cm^2)
0
5
10
15
20
25
0
25
50
75
100

Figure 5

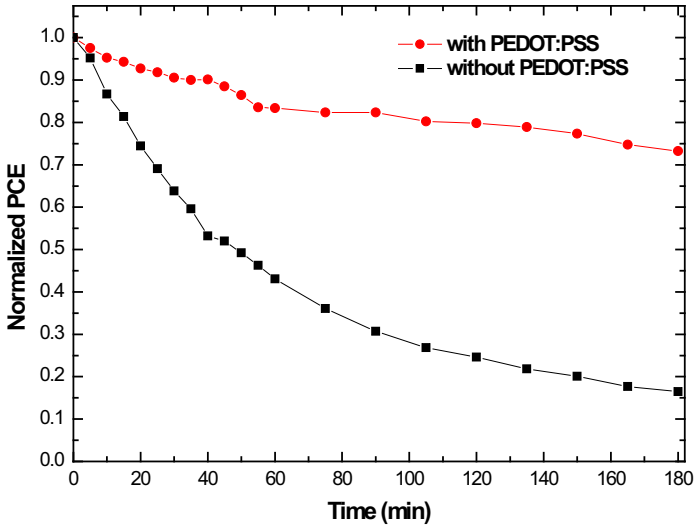

Figure 6a

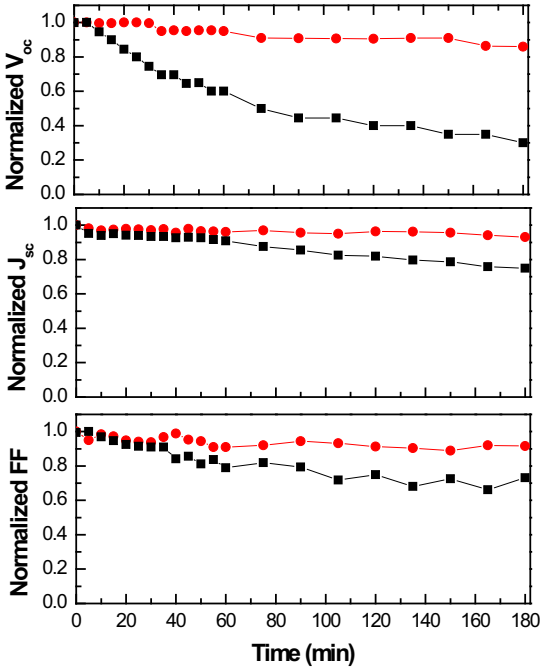

Figure 6b

Figure S1. High-resolution transmission electron microscopy image of PbSe QDs capped with oleate ligands. Scale bar: 5 nm. The average size of these PbSe QDs was ca. 5.5 ± 5 nm.

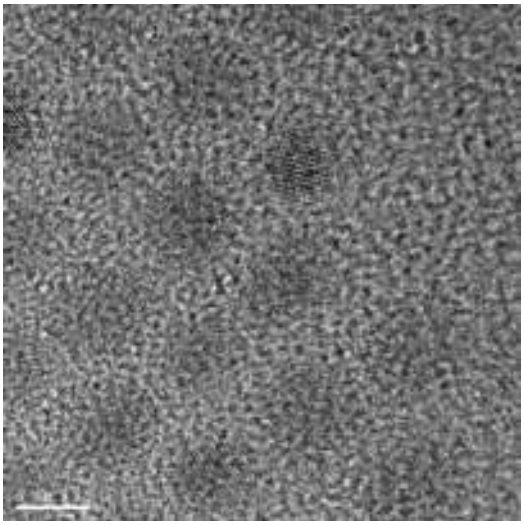

Figure S2. Plan-view scanning electron microscopy image of spin-cast PbSe QD films capped with (A) oleate and (B) butylamine ligands.

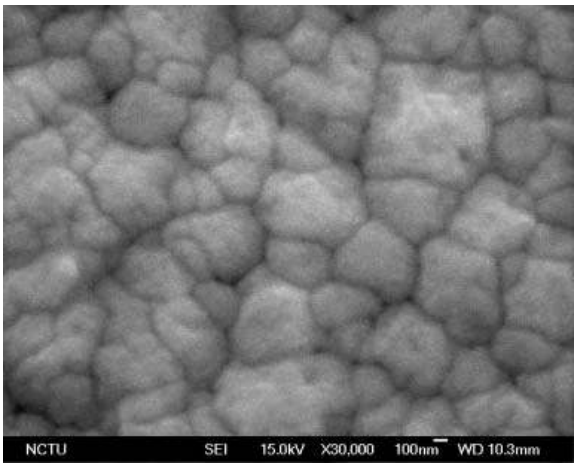

Figure S2A

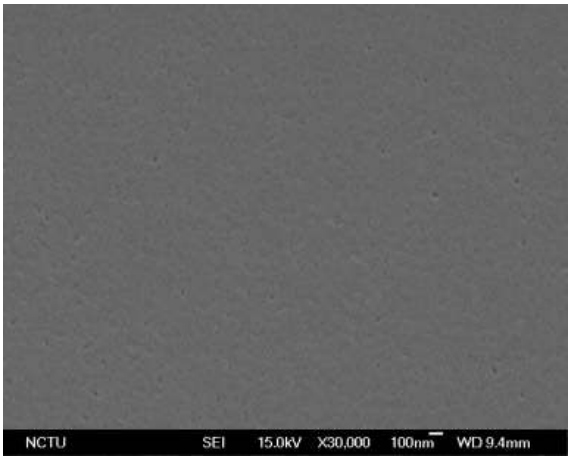

Figure S2B

Figure S3. Fourier transform infrared spectra of PbSe QD films: (i) oleate-capped, (ii) butylamine-exchanged, and (iii) butylamine-exchanged with subsequent 0.01 M EDT treatment.